Available online at www.sciencedirect.com
SCIENCE DIRECT®
PERGAMON
Acta Astronautica 54 (2004) 547–558
ACTA ASTRONAUTICA
www.elsevier.com/locate/actaastro

Experimental status of thrusting by electromagnetic inertia manipulation☆

Hector H. Brito

Instituto Universitario Aeronáutico, Ruta 20, Km. 5.5, Córdoba X5010JMN, Argentina

Received 29 April 2002; received in revised form 25 February 2003; accepted 10 June 2003

Abstract

It has been shown in previous works that given suitable charge and current distributions, the electromagnetic (EM) field can modify the inertial properties of the generating device if Minkowski's energy–momentum tensor holds for the description of field–matter interactions. The possibility then arises of obtaining mechanical impulses on the device, not undergoing any exchange of mass–energy with the surrounding medium, by EM inertia manipulation (EMIM). The aim of this paper is to present the accumulated experimental evidence about that means of achieving thrust. Three test series performed during the periods 1993–1997 and 1999–2000 on different experimental setups, are reviewed from the viewpoint of an identification of systematic spurious effects. A fourth series of tests recently conducted yields results that can hardly be explained without the EMIM mechanism. However, they are in contradiction with null results predicted by the currently admitted formulation of global EM forces. Further progress along this line of research will likely require improved test and measurement procedures, to get rid of residual spurious effects. Enhanced reliability of the reported results is also expected to arise from independent confirmation by other researchers.

1. Introduction

Either to go to the stars or, more pragmatically, to substantially cut down space transportation costs, new propulsion mechanisms must be found which get rid of propellants and/or conventional external assistance, i.e., the mythical "space drive" must still be invented [1]. This formally translates into the problem of achieving "jet-less" propulsion of spaceships that can then be seen as closed systems, i.e., without external assistance or mass/energy exchanges with the surrounding medium. As already shown, a formal solution to the problem does exist, provided the system is endowed with tensor mass properties [2]. The mass tensor formulation shows that the propulsion effect is to be related to the deviatoric part of the tensor, which exhibits the particularity of producing a non-vanishing linear momentum in the spaceship comoving Lorentzian frame. This has been found to be the case if static electromagnetic (EM) field momentum can develop in the rest frame of a physical arrangement of electric and magnetic sources including polarizable media.

Different theoretical answers are possible; they basically depend upon Abraham's and Minkowski's forms of the EM momentum density, as the three-dimensional expression of the so-called "Abraham–Minkowski controversy" about the correct

☆ Based on paper IAF-01-S.6.02 presented at the 52nd International Astronautical Congress, 1–5 October 2001, Toulouse, France.

E-mail address: hbrito@make.com.ar (H.H. Brito).

0094-5765/$ - see front matter © 2003 Elsevier Ltd. All rights reserved.
doi:10.1016/S0094-5765(03)00225-X

Nomenclature

$\boldsymbol{B}$	magnetic induction field
c_0	velocity of light in vacuum
c	velocity of light in arbitrary media
d	capacitor width
$\boldsymbol{D}$	electric displacement vector
E	magnitude of the electric field vector
$\boldsymbol{E}$	electric field vector
$\boldsymbol{f}$	electromagnetic force density
F	electromagnetic instantaneous thrust
$\mathbf{f}$	external 4-force
$\mathbf{F}$	thrust in 4-space
$\boldsymbol{g}$	three-dimensional momentum density
$\boldsymbol{G}$	global three-dimensional momentum
H	magnitude of the magnetic field vector
$\boldsymbol{H}$	magnetic field vector
I	total current
$\mathbf{I}$	identity 4-tensor
$\boldsymbol{j}$	density of current
m_{F}^{*}	mass of the field in the spaceship's rest frame
m_0	proper (rest frame) mass of the spaceship
$\mathbf{M}$	4-space mass tensor
n	number of turns
$\mathbf{p}_{\mathrm{F}}$	"propulsion field" 4-momentum
$\boldsymbol{s}$	energy flow
t	time
$\mathbf{v}$	4-velocity of the "solidification point"
V	3-dimensional region, volume, voltage
w	energy density
$\boldsymbol{x}$	location vector in 3-dimensional space
ε	dielectric constant
μ	magnetic permeability
ρ	density of charge
τ	proper (rest frame) time
ϕ	current–voltage phase shift
ω	angular frequency

Subscripts

0	at rest, in vacuum
i	induced field
r	relative

Superscripts

A	Abraham's
f	field
m	matter, mechanical
M	Minkowski's
S	standard

energy–momentum tensor of EM fields in polarizable media [3]. The controversy, lasting since 1909, strikingly remains as a yet unsolved issue of physics [4,5]. Supporters on the theoretical aspect split about equally between the two forms, according to literature reviews, while existing experimental evidence does not allow definite conclusions to be drawn.

In previous works, Minkowski's formalism was shown to allow for non-zero static EM field momentum, i.e., given suitable charge and current distributions, the inertial properties of the generating device can be modified by electromagnetic means, giving rise to the possibility of obtaining mechanical impulses on the device, not undergoing any exchange of mass–energy with the surrounding medium. A propulsion concept based upon this kind of inertia manipulation mechanism was subsequently drawn and the experimental setup built to test that concept was discussed, as well as the results obtained and the applied signal processing techniques [6,7]. Throughout this paper the theoretical bases as well as the experimental work are reviewed, together with new results gathered during a fourth test series carried out with a setup configuration assuring "closed system" operation.

2. Thrust by EM inertia manipulation

2.1. The single-particle system approach

Studies about inertia as something that could be manipulated for propulsion purposes are not new, and a tentative explanation has already been undertaken on the basis of the relativistic mechanics of extended bodies under electrostatic pressures [8]. However, the Covariant Propulsion Principle (CPP), as proposed in

Ref. [2], allows for a general formulation of the problem, provided a "propulsion field" of 4-momentum $\mathbf{p}_F$ can be ascribed to the whole system, analog to the ejecta subsystem appearing in rocket propulsion. The system can then be viewed as a single particle located at the "matter" system c.m. (or any "structural" point) so that a mass tensor is readily found as related to the whole system which reads in geometric notation

$$\mathbf{M} = (m_0 + m_F^*)\mathbf{I} + (\mathbf{p}_F \wedge \mathbf{v})/c_0^2. \tag{1}$$

For a closed system ($\mathbf{f} = \mathbf{0}$),

$$\mathrm{d}(\mathbf{M}\cdot\mathbf{v}) = \mathbf{0} \Rightarrow \mathbf{M}\cdot\mathrm{d}\,\mathbf{v} = -\mathrm{d}\,\mathbf{M}\cdot\mathbf{v}. \tag{2}$$

The 4-acceleration of the chosen "solidification point" now becomes

$$m_0\,\mathrm{d}\,\mathbf{v} = -(\mathrm{d}\,\mathbf{p}_F \wedge \mathbf{v})\cdot\mathbf{v}/c_0^2. \tag{3}$$

Eq. (3) shows that to have zero "matter" 4-acceleration for any 4-velocity, ($\mathrm{d}\mathbf{p}_F \wedge \mathbf{v}$) must vanish, i.e., the deviatoric part of the mass tensor variation must vanish. It is also shown that this comes out as a sufficient condition for vanishing acceleration. Thus, the 4-thrust on the single particle, in any arbitrary frame, is given by

$$\mathbf{F} = -\frac{\mathrm{d}\mathbf{p}_F}{\mathrm{d}\tau}. \tag{4}$$

Eq. (4) expresses, as expected, the law of conservation of the total system energy–momentum, consistently with Eq. (2). The change of the mechanical (matter) momentum exactly balances the change of the propulsion field momentum; momentum is then being exchanged within the whole closed system. The device works as a propulsion field momentum "accumulator" whereas the mechanical momentum that can be drawn from it is, by present physics paradigms, limited to the propulsion field momentum amount.

2.2. Electromagnetic field momentum

Since thrust must be related to the time change of a propulsion field momentum, the question arises about the general existence conditions of momentum of electromagnetic origin in the "matter" comoving frame. A fully covariant formulation of the problem requires to consider the energy–momentum tensors for a closed physical system consisting of "matter" and EM fields. By applying the Law of 4-Momentum Conservation to the particles and fields contained in any four-dimensional region of space–time bounded by a closed, three-dimensional surface, the system 4-momentum is found, for closed systems, to be conserved in time. Now, if the observer's frame coincides with the frame where the "matter" is at rest when no EM field is present, the condition for anisotropic mass tensor when the EM field is ON, means that in no case the system 4-momentum aligns with the observer's 4-velocity [6]. These are global consequences of mass tensor anisotropy.

When consideration is given to the locality of the energy–momentum conservation law, the following relationship can be found for the volume integral G of the momentum densities, when the fields die out rapidly at infinity [9]

$$\int_V (\boldsymbol{g}^{(\mathrm{m})} + \boldsymbol{g}^{(\mathrm{f})})\,\mathrm{d}V = -\int_V \boldsymbol{x}\, div\,(\boldsymbol{g}^{(\mathrm{m})} + \boldsymbol{g}^{(\mathrm{f})})\,\mathrm{d}V. \tag{5}$$

By introducing the relationship between the energy flow and the momentum density, and assuming that Planck's principle of inertia of the energy does not necessarily hold for the EM energy flux, Eq. (5) becomes

$$\int_V (\boldsymbol{g}^{(\mathrm{m})} + \boldsymbol{g}^{(\mathrm{f})})\,\mathrm{d}V = -\int_V \boldsymbol{x}\, div\left(\frac{\boldsymbol{s}^{(\mathrm{m})}}{c_0^2} + \frac{\boldsymbol{s}^{(\mathrm{f})}}{c^2}\right)\mathrm{d}V, \tag{6}$$

or,

$$\int_V (\boldsymbol{g}^{(\mathrm{m})} + \boldsymbol{g}^{(\mathrm{f})})\,\mathrm{d}V = \int_V \frac{\boldsymbol{x}}{c_0^2}\left[\frac{\partial w}{\partial t} - grad\left(\frac{c_0}{c}\right)^2\cdot\boldsymbol{s}^{(\mathrm{f})} + \left(\frac{c_0^2}{c^2} - 1\right) div\,\boldsymbol{s}^{(\mathrm{f})}\right]\mathrm{d}V. \tag{7}$$

2.3. Transient regimes

It can be seen that to obtain non-zero total momentum for specific matter–field configurations, a non-vanishing energy density variation rate is a sufficient condition. It is a sufficient condition for any matter–field configuration, provided Planck's principle of inertia holds within polarizable matter too. Mass tensor anisotropy, as related to a special frame, can thus arise when net mass–energy fluxes take

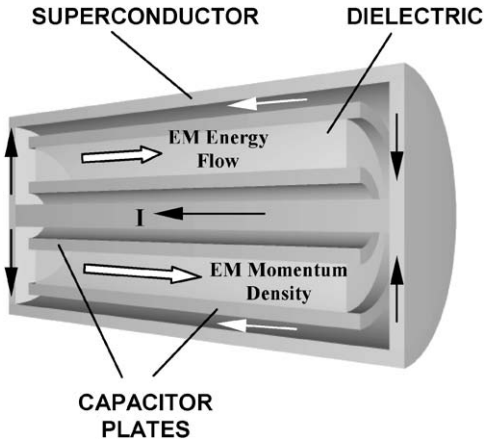

Fig. 1. Stationary regime in the 'matter' rest frame with polarizable media.

place within closed systems where Planck's principle of inertia holds everywhere, or, in other words, when the system is under anisotropic non-equilibrium conditions.

2.4. Stationary regimes

For stationary regimes and any matter–field configuration Eq. (7) becomes

$$\int_V \boldsymbol{g}^{(\mathrm{f})}\,\mathrm{d}V = -\int_V \boldsymbol{x}\left[grad\left(\frac{1}{c^2}\right)\cdot \boldsymbol{s}^{(\mathrm{f})} + \left(\frac{1}{c^2}\right) div\,\boldsymbol{s}^{(\mathrm{f})}\right]\mathrm{d}V. \tag{8}$$

The quantity between brackets being $\mathrm{div}\,\boldsymbol{g}^{(\mathrm{f})}$, a non-zero LHS is possible provided $\boldsymbol{g}^{(\mathrm{f})}$ is not divergence-free everywhere. This can be achieved for arbitrary matter–field configurations if gradients of EM wave propagation group velocity occur in the integration region, i.e., as assumed for the derivation of Eq. (7), Planck's principle of inertia does not hold within polarizable media, in which case the energy–momentum tensor becomes unsymmetrical. This is the case for the setup shown as a cutaway in Fig. 1; it consists of a permanently charged cylindrical capacitor with high ε dielectric, housed into a superconductor made cylindrical box with a central column. A previously set current, flows meridianly on the cylindrical walls of the box, radially on the circular ones and back through the column to close the three-dimensional circuit. It can be seen that $div\,\boldsymbol{s}^{(\mathrm{f})} = 0$ everywhere (no electrical power sources) and a non-vanishing total EM momentum can only arise from the RHS first term of Eq. (8). The contributions for the volume integral come from the free surfaces of the dielectric, through which jumps of the velocity of light take place in the direction of the EM energy flux.

For this particular setup, transient regimes do not allow to produce an EM momentum contribution since the energy density variation rates distribute symmetrically throughout the setup regions.

2.5. The Abraham–Minkowski connection

The existence conditions for stationary regimes are consistent with the use of Minkowski's energy–momentum tensor for the EM field [3]. By definition, the Relativistic Mechanics Laws of Conservation are satisfied; the same is true, nevertheless, for the Abraham's energy–momentum tensor, together with other forms of the electromagnetic energy–momentum tensor. This is precisely the still-standing [4,5] Abraham–Minkowski controversy about the form of that energy–momentum tensor, specially for low-frequency or quasi-stationary fields [3,10–12]. It reduces, basically, to the discrepancy about the mathematical expression of the EM momentum density:

$$\text{Abraham's claim}: \quad \boldsymbol{g}^{\mathrm{A}} = \frac{(\boldsymbol{E}\times\boldsymbol{H})}{c_0^2}, \tag{9}$$

$$\text{Minkowski's claim}: \quad \boldsymbol{g}^{\mathrm{M}} = (\boldsymbol{D}\times\boldsymbol{B}). \tag{10}$$

Abraham's expression is fully consistent with Planck's principle of inertia, since $\boldsymbol{E}\times\boldsymbol{H}$ represents the EM energy flow, whereas Minkowski's is not. The issue is thus highly relevant to "propellantless" propulsion, since the resultant total EM 4-momentum acts exactly as the generic propulsion field $\mathbf{p}_{\mathrm{F}}$ in Eq. (5), so EM inertia manipulation becomes a theoretical possibility. Experiments to definitely settle the question are still needed since some partly achieved attempts [13–16] have led to inconclusive results. A positive answer in favor of Minkowski's EM tensor would allow "jet-less" propulsive effects by EM fields manipulation.

3. Alternating thrust experiments

A propulsion concept based upon the EM inertia manipulation mechanism has subsequently been produced. It basically consists of suitably grouping the sources of electric and magnetic fields within a rigidly connecting device, as depicted in Fig. 1. By doing so, a stationary Minkowski's EM field momentum can develop owing to the dielectric filled region; by controlling the intensities of these fields, the inertia properties of the system as a whole, when represented by its "matter" part—the device—, are allowed to change so that a conversion of the EM field momentum into mechanical momentum of the device is expected to happen, and reciprocally, again if Minkowski is right. Nevertheless, it must be realised that this device works as an EM momentum "accumulator". The mechanical momentum that can be drawn from is, in accordance with present physics paradigms, limited to the "accumulated" EM momentum amount.

3.1. Experimental setup rationale

An electromagnetic momentum generator (EMMG), based on the schematics of Fig. 2, the two-dimensional and conventional conductors version of Fig. 1, was engineered up to the "proof of concept" level and an experiment was designed aimed to verify that: (a) The Minkowski's EM energy–momentum tensor does describe properly the electromagnetic field–matter interactions in polarizable media. (b) Global EM momentum in the matter rest frame of a closed system is being generated, or, equivalently for such a system, a non-scalar 4-mass tensor behavior is being obtained. (c) The experimental thruster is applying mechanical forces on the test stand without expenditure of mass, besides that equivalent to the radiant energy

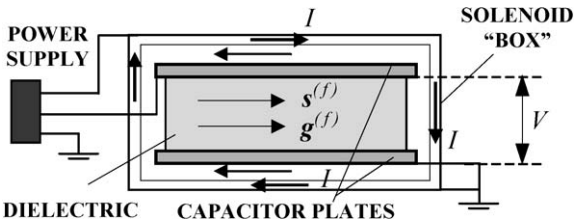

Fig. 2. EM momentum generator schematics.

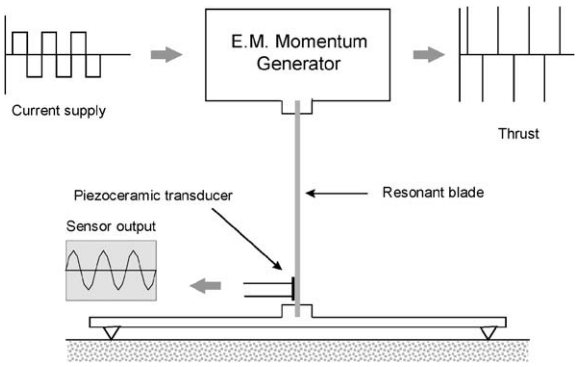

Fig. 3. Micromotion sensing concept.

dissipated from the system (e.g., Joule heating), which cannot account for the observed effects.

An experimental setup was accordingly implemented which consists of mounting the device as a seismic mass atop a mechanical suspension, as shown in Fig. 3. A supply of 6 A AC (square wave) to three 900 turns parallel mounted toroidal coils and 4 kV DC to three parallel mounted 10 nF, 8 mm wide annular capacitors, with $BaTiO_3$ ceramic dielectrics ($\varepsilon_r \approx 5700$), allows for a total EM momentum amplitude (square wave) around 10^{-8} Ns, as calculated by means of Eq. (10). The alleged conversion of Minkowski's EM momentum into mechanical momentum of the EMMG generates in turn forces acting upon this device. By means of a square wave activation of the device at a frequency close to the fundamental frequency of the seismic suspension, the supporting blade of the test fixture can be made to resonate so an amplified upper end displacement response is obtained.

Displacements in the range 10^{-8}–10^{-7} m were to be expected for 5 Hz resonant conditions. Piezoceramic strain transducers (PZTs) were devised to detect this range of displacements, taking into account technological as well as financial constraints. The output voltages of the PZTs is proportional to the strain level in a broad dynamic range, achieving sensitivities (seismic and acoustic threshold in controlled environments) up to 10^{-11} m/m [17]. This is two orders of magnitude lower than the expected levels, as related to the sensing fixture shown in Fig. 3. However, the full signal includes ground- and environment-induced noise as observed in preliminary testing. This

microseismic excitation can account for displacements comparable to those expected to be caused by the investigated effect, with a narrow band frequency response centered in the first natural frequency of the sensing fixture.

Another source of unwanted noise is the residual interaction between the coils and the Earth magnetic field, which can account for equally comparable total displacements, albeit with a deterministic distribution in the frequency domain. A third source of noise relates to the magnetic interaction between the moving and the fixed parts of the AC and DC circuits (self-magnetic interaction), those belonging to the device atop the resonant blade and to the external power supply, respectively. It was also found to contribute to the displacements on practically the same level as the two above mentioned sources, but at twice the coil activation frequency.

Other sources of noise have been considered, too, like air motion, electrostatic couplings, sound, radiometric effects, spherics, etc. which can have a degrading effect on the measurements quality, although to a lesser extent than the forementioned sources. The overall estimated effect amounts to $-60\ \text{dB} < \text{S/N} < -40\ \text{dB}$ at the transducer output and the need for further processing arises. To this aim, the analog transducer output signal is digitized through a 12-Bit data acquisition board, making it available to PC-based storage devices.

3.2. Test implementation and philosophy

Two series of tests were conducted during the period 1993–1997. Only one measurement channel was available during the first series of tests, with no vibration isolation provisions. The second test series included, besides the main transducer measurement channel, a dummy seismic fixture with its transducer and measurement channel, a voltage supply measurement channel, and a vibration-free table. In both series data were acquired in sequences of 5000 samples at a rate of 500 samples/s. Power Spectral Density (PSD) using Welch's averaged periodogram method was estimated over a 2048 length frequency interval. The test philosophy was based upon comparison of results in the frequency domain, due to different excitation schemes. These were: (A) Ground-induced noise. (B) Coils ON, capacitors OFF + (A). (C) Coils ON, capacitors ON + (A). (D) Coils OFF, capacitors ON + (A).

Following modeling and simulation activities, geomagnetic and self-magnetic interaction noises were expected to appear in (B) and (C) as compared to (A), while the influence of the capacitors should appear in (C) as compared to (B) if thrust by inertia manipulation is acting upon the device; no difference was expected to arise between (D) and (A), since static electric fields alone cannot account for the vibratory behavior of the sensing fixture.

3.3. Results assessments

Results corresponding to both series were reported in Refs. [6,7], where, as expected, differences have been observed between the (A) and (B) spectra, mainly caused by geomagnetic noise. Differences have also been observed between the (A) and (C) spectra, but slight differences between the (B) and (C) spectra, while intriguing, cannot be fully ascribed to the alleged EMIM effect, since they tend to fade out following statistical averaging of the spectra. Again, as expected, no substantial differences have been observed between the (A) and (D) spectra.

Since a significant amount of ground-induced noise was also observed during the second test series, in spite of the improved setup as mentioned before, it was also decided to proceed to intensive signal processing so as to achieve a higher confidence in the electro-magnetic inertia manipulation (EMIM) effect detection. Data gathered during the second series of tests, were firstly processed to carry on a system identification on the basis of the ground motion excitation only. An auto regressive moving average (ARMA) model structure was then identified; later, inverse filtering was performed for every output sequence in order to obtain the equivalent ground motion; then, filtering by the vibration isolation fixture led to the reconstruction of the sensing device base motion; finally, optimal filtering (Wiener filter) was performed on the resultant output, using the EMMG-induced excitation as the "desired" signal.

Raw data show, after processing, a more accurate spectral structure as related to the sought excitation spectrum which consists of equal amplitude odd harmonics of the square wave fundamental frequency,

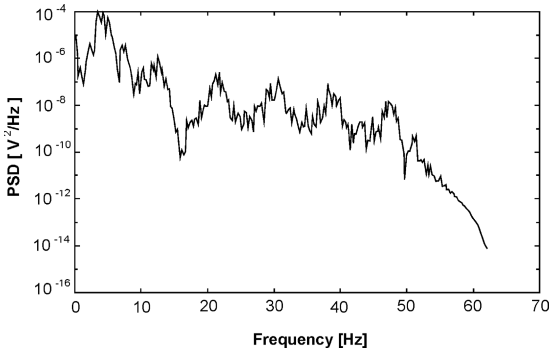

Fig. 4. Second test series PSD—case (A).

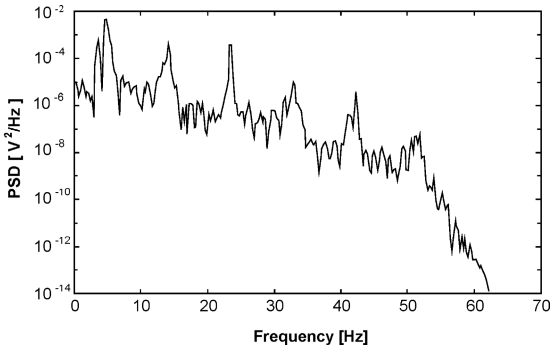

Fig. 5. Second test series PSD—case (B).

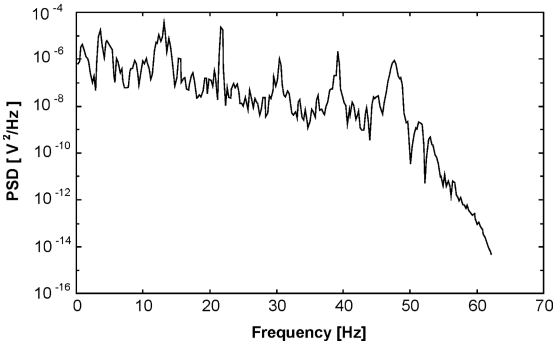

Fig. 6. Second test series PSD—case (C).

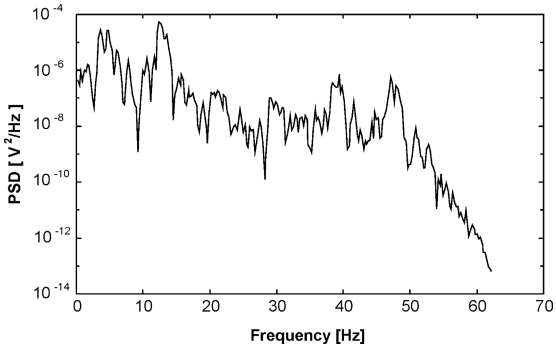

Fig. 7. Second test series PSD—case (D).

as shown in Fig. 4. Spectrum (A) contains low-level residuals induced by the Wiener filter—a sort of numerical artifact—as well as spectrum (D) (Fig. 7). Spectrum (B) (Fig. 5) does not match the "message" spectrum, it better fits that of the geomagnetic noise square wave excitation.

Spectrum (C) (Fig. 6) shows a structure which suggests an alternating impulsive excitation, as would be the case when a square wave EM field–matter momentum exchange is present.

The figures are representative of around 16 sequences per case. Statistical analysis over the whole data set has already been carried out and individual differences have been found to average out within the standard deviation of either spectra (B) or (C). The use of adaptive noise cancellation procedures was foreseen too, either on the raw output data or on the inverse filtered output data [18–20]. Preliminary work has been carried out on this subject but no definite results are available as to date, the involved numerical techniques requiring further refinement.

4. Sustained thrust experiments

Notwithstanding the improvements implemented on the second test series, uncertainties still remained which could account for the observed "positive" results, regarding especially to:

(a) Geomagnetic influence.
(b) Numerical artifact as in Figs. 4 and 7.
(c) Colored ground noise centered around the excitation frequency.
(d) Air motion (ionic wind).
(e) Power supply induced EMI.

In order to get rid of these interfering effects, the experiment was modified during 1999, according to an

alternative formulation of the Abraham–Minkowski controversy, this time in terms of force densities. By assuming a non-dispersive, isotropic medium, the force densities become [3,21]

$$\boldsymbol{f}^{\mathrm{M}} = \rho\boldsymbol{E} + \boldsymbol{j} \times \boldsymbol{B} - \tfrac{1}{2} E^2 \nabla\varepsilon - \tfrac{1}{2} H^2 \nabla\mu, \tag{11}$$

$$\boldsymbol{f}^{\mathrm{A}} = \boldsymbol{f}^{\mathrm{M}} + \frac{\varepsilon_r \mu_r - 1}{c_0^2} \frac{\partial}{\partial t} (\boldsymbol{E} \times \boldsymbol{H}). \tag{12}$$

These force densities clearly differ inside matter for generic fields; they are however identical for static fields, irrespective of the medium. If harmonic fields are considered, the instantaneous values of the force densities differ, but their averaged values become identical and therefore useless for discriminating between the two formulations. This is the reason Walker & Walker's claim [15] favoring Abraham's one is essentially wrong and the experiment remains inconclusive.

The EM inertia manipulation (EMIM) experiment was modified in such a way that both $\boldsymbol{D}$ and $\boldsymbol{B}$ fields were subjected to harmonic evolution. The averaged effect of the total EM force was sought, so Eq. (11) must be used for its theoretical estimation as applied to the schematics of Fig. 2, with AC voltage supply to the capacitor. This estimation was carried out in Ref. [7] by neglecting capacitor edge effects, by considering the coils as a conducting "box" bearing a negligible voltage w.r.t. to the capacitor plates and by assuming that the polarization current within the dielectric contributes to the second term of Eq. (11).

As a result, electric self-interaction, represented by the first term of Eq. (11) and magnetic self-interaction represented by the second term of the same equation, simply cancel out. Since non-magnetic matter is involved, contribution to the total EM force acting upon the device comes from the third term. This contribution is non-zero through the boundaries of the dielectric filled volume due to the induced electric fields of magnitude E_i appearing on these boundaries. They yield an unbalancing effect on the electric field of magnitude E set by the capacitor, so the integrated effect does not cancel out in the $\boldsymbol{E} \times \boldsymbol{H}$ direction.

Application of the formula for a parallel plate capacitor of width d, Lenz's Law and Ampere's Law for an infinite length solenoid of n turns, yields the following expression for the EM instantaneous thrust, as a function of the harmonic voltage $V \sin \omega t$ on the capacitor and the harmonic current $I \sin(\omega t + \phi)$:

$$F = -\frac{\varepsilon_r \varpi n I V d}{c_0^2} \left(\frac{1}{2} \sin 2\varpi t \cos\varphi - \sin^2 \varpi t \sin\varphi \right). \tag{13}$$

The averaged value then results

$$\langle F \rangle = \frac{\varepsilon_r \varpi n I V d}{2 c_0^2} \sin\varphi \tag{14}$$

with maxima at $\varphi = \pm\pi/2$. The results obtained with Walker & Walker's experiment are consistent with this formulation and can, as the authors readily did, be interpreted in terms of the polarization current contribution to the Lorentz force [15].

However, Eq. (14) must be seen as a conflicting result if total momentum must be conserved, as stated previously. In fact, the standard treatment of the problem requires the polarization current to be excluded from the magnetic contribution to the Lorentz force, the self-magnetic interaction does not cancel out and the second term of Eq. (13) must be corrected as follows:

$$F_{(2)} = -\frac{\varepsilon_r \varpi n I V d}{c_0^2} \times \left(\frac{1}{2} \sin 2\varpi t \cos\varphi + \cos^2 \varpi t \sin\varphi \right), \tag{15}$$

so the total "standard" force is

$$F^S = -\frac{\varepsilon_r \varpi n I V d}{c_0^2} (\sin 2\varpi t \cos\varphi + \cos 2\varpi t \sin\varphi) \tag{16}$$

and the averaged value goes to zero.

Without the polarization current (Roentgen current) contribution, Walker & Walker's positive results can only be explained in terms of induced electric forces on the free charges sitting on the capacitor plates, in which case Kelvin forces develop in the dielectric that amount to exactly the opposite of the former. The EM force density derived from the Einstein–Laub energy–momentum tensor includes the Kelvin contribution and predicts a null instantaneous torque on the capacitor as a whole [3,15]. Moreover, azimuthal electric fields are not consistent with the corresponding boundary conditions on annular conducting plates.

Therefore, the modified EMIM experiment should allow discriminating between the "standard" and the

presently proposed formulation of the averaged EM force. To take advantage of the sensing device characteristics, the voltage supply to the capacitor is reversed at a frequency much lower than the common power supply frequency, so the seismic setup is put into vibratory motion if the "proposed" formulation is correct. By doing so, the interfering effect (a) becomes averaged out at zero; direct detection also allows overcoming the interfering effect (b) since no Wiener filtering is necessary; moreover, if the voltage reversing frequency is different from the setup natural frequencies, the interfering effect (c) becomes less significant. Regarding ambient air motion (d), two sources of interference are considered: d1) gradient (thermal, pressure) forced airflow, and d2) voltage gradient induced airflow (electric wind). Type (d1) sources are present even in controlled room environment, although it is highly unlikely that they could bear an oscillatory behavior such as aerodynamic forces act upon the device with the right frequency. Type (d2) interferences are known to be proportional to voltage differences between conductors in partially conducting media [22–24]. Therefore, the voltage supply being subjected to harmonic evolution, they also average out at zero. Uncertainties are expected to remain regarding interfering effect (e).

4.1. Third test series

Experiments were performed according to the test philosophy of the preceding test series. The hardware configuration with the device atop the resonant blade and external power supply was also kept for this test series. The supply or "carrier" frequency was set at 30 kHz; a 30 Hz reversing frequency was initially applied and propulsive effects show up only when the Caps ON–Coils ON condition holds. Furthermore, maxima are obtained for a voltage–current phase shift of 90°, as predicted by the proposed formulation. A comparison of case (C) results with the corresponding simulation results (dotted line) is shown in Fig. 8, where a close agreement is found for the response to the alleged EMIM averaged force at 30 Hz reversing frequency. A comparison between cases (A) and (C) is shown in Fig. 9.

Phase shift dependence is shown in Fig. 10, where experimental PSD peak values at 27 Hz are plotted versus the voltage–current shift angle. A reversing

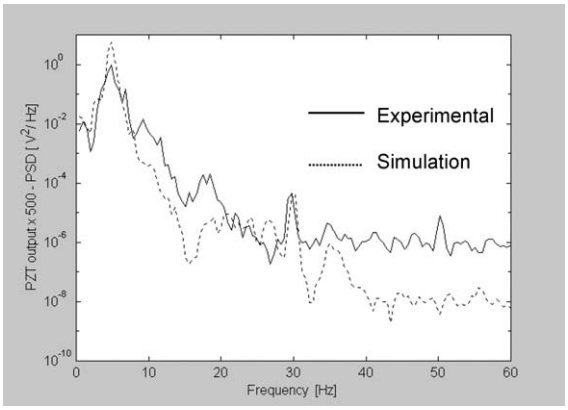

Fig. 8. Third test series—Case (C) experimental and simulation results.

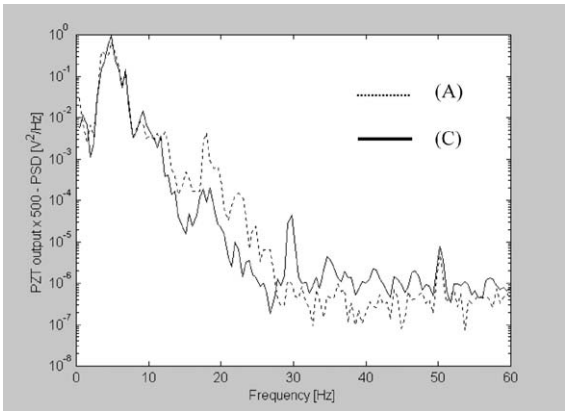

Fig. 9. Third test series—Cases (A) & (C).

frequency lower than 30 Hz was selected to take advantage of better setup transmissibility for all shift angles, just before entering the noisy region of the spectrum. PSD peak values at each angle show some amount of spreading; this effect was initially thought to be due to contributions of magnetic interactions between the capacitor and the coil circuits during non-synchronized voltage reversings and/or between the capacitor circuit and the geomagnetic field. However, order of magnitude estimations show those interactions to be unable to account for the observed deviations. Their source remains unknown, so far, except for fluctuations of ground noise components at the reversing frequency. Nevertheless, a slightly

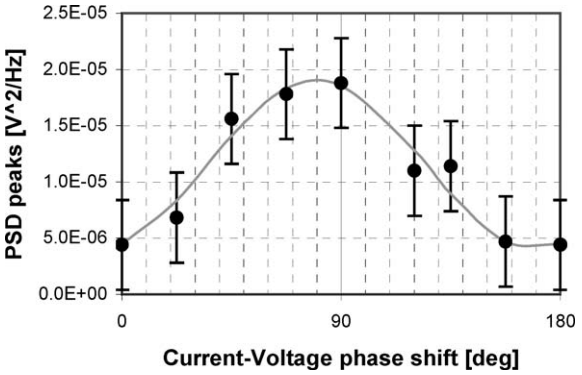

Fig. 10. Third test series average PSD peak values at 27 Hz, with 90% confidence intervals.

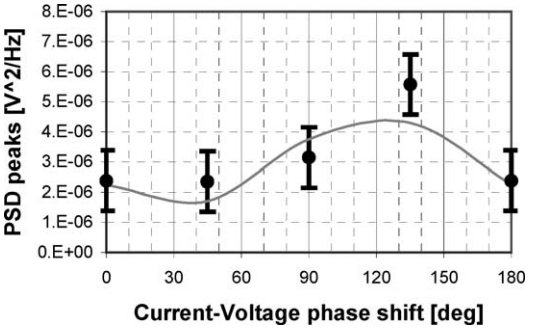

Fig. 11. Fourth tests series average PSD peak values at 32 Hz, with 90% confidence intervals.

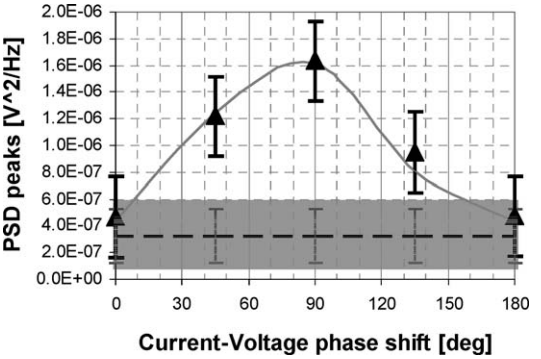

Fig. 12. Fourth tests series average PSD peak values at 32 Hz, with 90% confidence intervals (w.r.t. Caps ON–Coils OFF average PSD peak values).

shifted squared sine trend can clearly be seen to emerge from the plotted data.

4.2. Fourth test series

The hardware configuration was modified during spring 2000 so the device could be operated in a genuine "closed system" mode. Both the EMIM thruster and its Power Supply Unit were located and rigidly assembled atop the resonant blade of the sensing fixture. This would in principle allow to assess the influence of external wiring on the previous test series. However, due to the added seismic mass, the thrust stand dynamics were considerably altered and, so far, only qualitative analysis can be done. Fully quantitative assessments demand a thorough thrust stand characterization, which is currently underway.

The test philosophy remained the same and data were processed in the frequency domain, too. To assess the influence of the reversing frequency, tests have been carried out at 32 and 38 Hz. Cases (A) and (B) runs behaved as expected, qualitatively similar to the corresponding third test series data. Sharp spectral peaks show up in Case (C) runs, but, unexpectedly, spectral peaks show up in Case (D) runs, too, amounting to an order of magnitude comparable to (C) type peaks. This effect is likely to be due to the vibratory motion, at the reversing frequency, of a transformer casing in the secondary circuit of the capacitor's supply line. Absolute phase shift dependence at 32 Hz is shown in Fig. 11, while relative values taking into account the average peak values under Caps ON–Coils OFF conditions are shown in Fig. 12. The corresponding average "ground level" (Caps OFF–Coils OFF, dashed line) is also shown in the same figure, together with the 90% confidence intervals.

In spite of the forementioned voltage supply phenomenon, the residual levels allow a slightly shifted squared sine function fitting (the continuous curve is a smoothed fitting of true squared sine-dependent values at the experimental phase shift angles). A similar trend is observed for the 38 Hz reversing frequency but lesser shift angle values were available to date. PSD peak values are considerably higher than those obtained for 32 Hz, the same being true for the "ground level" at that frequency. It is speculated that these higher response levels may be related to the proximity of a natural frequency of the mechanical fixture.

5. Conclusions

The possibility of achieving thrust without reaction mass or beamed power, by means of EM inertia manipulation, has been reviewed. The importance of the electromagnetic momentum density expression has been emphasized as being the crucial issue of the continuing Abraham–Minkowski controversy. Experimental elucidation of the controversy was sought after and instrumented around a so-called EMIM force-producing device. It was also pointed out that within present physics paradigms, only limited action time propulsive forces can eventually be obtained.

Tests performed during the period 1993–1997, with slightly different instrumentation, produced results, which, after processing through spectral analysis, system modeling & identification and optimal filtering techniques, when applicable, consistently pointed to a mechanical vibration allegedly induced by mass/inertia manipulation of the device, or matter–electromagnetic field momentum exchange, as predicted by Minkowski's formalism. Along with the processing and analysis activities, other sources of vibration were taken into account, or removed when possible, according to a systematic error and disturbance (spurious effects) fighting procedure. However, no direct detection of the sought effect has been obtained up to now; the overall detectability of the experimental setup needs further improvements, jeopardized by several potentially interfering effects.

Third and fourth test series conducted since 1999 on a redesigned experiment, aiming to get rid of most of the identified spurious effects, yield comparatively sharper and clearer evidence of force-producing effects as predicted by the alternative formulation of global EM forces, albeit in contradiction with null results predicted by the "standard" formulation. Although positive results seem to indicate that the system momentum is not conserved, which casts severe doubts about their validity, a conclusive demonstration that this is absolutely forbidden by the laws of physics has not yet been given and future breakthroughs in understanding the nature of inertia and motion may lead to more optimistics prospects. Furthermore, the alternative formulation correctly predicts peer-reviewed results.

Meanwhile, work still remains to be done to validate these results, especially from the viewpoint of the effects of power supply induced EMI on the measurement channels, sharing the same spectral signature with the pursued effect. They are expected to be overcome by means of Laser Doppler Vibrometry techniques. Self-magnetic interactions in wiring and windings of power-supply components was also identified as an important source of mechanical noise. Although efforts have already been made to filter out its influence from the experimental data, safer results will be obtained by a substantial increase of power. This will allow the use of a reversing voltage frequency close to the fundamental frequency of the sensing fixture, for the alleged observable effect to show up well over the ground induced noise. Definite answers will indeed be provided by in-orbit testing, simultaneously getting rid of all mentioned interferences.

Acknowledgements

The author gratefully acknowledges the financial support of "Instituto Universitario Aeronautico" the National Agency for the Support of Science and Technology (Argentina)—ANPCyT (Grant FONCYT-PICT-99-10-07107) and Agencia Cordoba Ciencia.

References

[1] M.G. Millis, Challenge to create the space drive, Journal of Propulsion and Power 5 (1997) 577–582.
[2] H.H. Brito, A propulsion-mass tensor coupling in relativistic rockets motion, Proceedings of the Space Technology Applications International Forum (STAIF-98), (Part 3), Institute for Space and Nuclear Power Studies, Albuquerque, NM, 1998, pp. 1509–1515.
[3] I. Brevik, Experiments in phenomenological electrodynamics and the electromagnetic energy–momentum tensor, Physics reports 52 (3) (1979) 139.
[4] S. Antoci, L. Mihich, A forgotten argument by Gordon uniquely selects Abraham's tensor as the energy–momentum tensor for the electromagnetic field in homogeneous, isotropic matter, Nuovo Cimento B 112B (1997) 991–1007.
[5] F.S. Johnson, B.L. Cragin, R.R. Hodges, Electromagnetic momentum density and the Poynting vector in static fields, American Journal of Physics 62 (1994) 33–41.
[6] H.H. Brito, Propellantless propulsion by electromagnetic inertia manipulation: theory and experiment, AIP Conference Proceedings 458, American Institute of Physics, New York, 1999, pp. 994–1004.
[7] H.H. Brito, Research on achieving thrust by EM inertia manipulation, AIAA Paper 2001-3656, 37th AIAA/

ASME/SAE/ASEE Joint Propulsion Conference, Salt Lake City, Utah, July 2001.
[8] R. Marchal, Sur l'inertie électromagnétique, Comptes Rendus 268A (1969) 299–301.
[9] W.H. Furry, Examples of momentum distributions in the electromagnetic field and in matter, American Journal of Physics 37 (1969) 621–636.
[10] H.M. Lai, Electromagnetic momentum in static fields and the Abraham–Minkowski controversy, American Journal of Physics 48 (1980) 658–659.
[11] I. Brevik, Comment on "Electromagnetic momentum in static fields and the Abraham–Minkowski controversy", Physics Letters 88A (1982) 335–338.
[12] H.M. Lai, Reply to "Comment on electromagnetic momentum in static fields and the Abraham–Minkowski controversy", Physics Letters 100A (1984) 177.
[13] R.P. James, Force on permeable matter in time-varying fields, Ph.D. Thesis, Department of Electrical Engineering, Stanford University, 1968.
[14] G.B. Walker, D.G. Lahoz, G. Walker, Measurement of the Abraham force in barium titanate specimen, Canadian Journal of Physics 53 (1975) 2577–2586.
[15] G.B. Walker, G. Walker, Mechanical forces in a dielectric due to electromagnetic fields, Canadian Journal of Physics 55 (1977) 2121–2127.
[16] D.G. Lahoz, G.M. Graham, Observation of electromagnetic angular momentum within magnetite, Physical Review Letters 42 (1979) 1137–1140.
[17] R.L. Forward, Picostrain measurements with piezoelectric transducers, Journal of Applied Physics 51 (1980) 5601–5603.
[18] B. Widrow, et al., Adaptive noise cancelling: principles and applications, Proceedings of the IEEE 63 (12) (1975) 1692–1716.
[19] J.G. Proakis, C.M. Rader, F. Ling, C.L. Nikias, Advanced Signal Processing, Macmillan Publishing Co., New York, 1992, pp. 315–399.
[20] DSP Design and Simulation Using the SIMULINK DSP Blockset, SIMULINK Technical Computing Brief, The Mathworks Inc., Natick, MA, 1996.
[21] B.C. Eu, Statistical foundation of the Minkowski tensor for ponderable media, Physics Review A 33 (1986) 4121–4131.
[22] S.I. Cheng, Glow discharge as an advanced propulsion device, ARS Journal 12 (1962) 1910–1916.
[23] L.B. Loeb, Electric Coronas, Their Basic Physical Mechanisms, University of California Press, Berkeley, CA, 1965.
[24] E.A. Christensen, P.S. Moller, Ion-neutral propulsion in atmospheric media, AIAA Journal 5 (10) (1967) 1768–1773.